NISTIR 6463

Model Phase Diagrams For an FCC Alloy

R. J. Braun
J. Zhang

Department of Mathematical Sciences
University of Delaware
Newark, DE 19716, USA

J. W. Cahn
G. B. McFadden

U. S. DEPARTMENT OF COMMERCE
Technology Administration
National Institute of Standards
and Technology
Gaithersburg, MD 20899

A. A. Wheeler

Faculty of Mathematical Studies
University of Southampton
Highfield, Southampton, SO17, 1BJ, UK

NIST
National Institute of Standards and Technology
Technology Administration
U.S. Department of Commerce

NISTIR 6463

Model Phase Diagrams For an FCC Alloy

R. J. Braun
J. Zhang

Department of Mathematical Sciences
University of Delaware
Newark, DE 19716, USA

J. W. Cahn
G. B. McFadden

U. S. DEPARTMENT OF COMMERCE
Technology Administration
National Institute of Standards
and Technology
Gaithersburg, MD 20899

A. A. Wheeler

Faculty of Mathematical Studies
University of Southampton
Highfield, Southampton, SO17, 1BJ, UK

January 19, 2000

U.S. DEPARTMENT OF COMMERCE
Norman Y. Mineta, Secretary

TECHNOLOGY ADMINISTRATION
Dr. Cheryl L. Shavers, Under Secretary
of Commerce for Technology

NATIONAL INSTITUTE OF STANDARDS
AND TECHNOLOGY
Raymond G. Kammer, Director

MODEL PHASE DIAGRAMS FOR AN FCC ALLOY

R.J. BRAUN AND J. ZHANG*
Department of Mathematical Sciences, University of Delaware, Newark, DE 19716, USA

J.W. CAHN AND G.B. MCFADDEN
National Institute of Standards and Technology, Gaithersburg, MD 20899, USA

A.A. WHEELER
Faculty of Mathematical Studies, University of Southampton, Highfield, Southampton, SO17 1BJ, UK

We describe a mean field free energy model that allows the computation of realistic phase diagrams for a particular set of ordering transitions in face centered cubic (FCC) binary alloys. The model is based on a sixth-order Landau expansion of the free energy function in terms of the three nonconserved order parameters that describe ordering on the underlying FCC lattice. When combined with appropriate gradient energy terms, this model will allow the self-consistent calculation of energetic and kinetic anisotropies of phase boundaries in future work.

1 Introduction

Equilibrium states of crystalline solids can undergo a variety of phase transitions as the temperature and concentration of the material is varied [1]. In this paper we will be concerned with order-disorder transitions for a face centered cubic (FCC) binary alloy that is composed of A and B atoms. In such a transition, the structure and spacing of the underlying lattice remains unchanged, but the arrangements of the A and B atoms on the lattice sites can vary with temperature and concentration. For this purpose the FCC lattice can be regarded as consisting of four interpenetrating simple cubic sublattices. The origin of one sublattice can be taken as the corner site of a unit cell and that of each of the other three sublattices is centered on one of the faces (see Fig. 1). At high temperatures, but below the melting point, the equilibrium state is typically a disordered phase, where the ratio of A and B atoms on each sublattice is the same. The structure is FCC and the four sublattice are equivalent by the symmetry of the FCC lattice. At lower temperatures, ordered phases can be favored, in which case there is a symmetry breaking. For the bulk ordered phases we consider here, the ratio of A and B atoms are uniform on each sublattice, but the ratio varies from sublattice to sublattice. An example of such an ordered phase occurs in the copper-gold system, in which the Cu_3Au phase at concentrations near 25% Au consists of gold atoms preferentially occupying one sublattice, which for convenience is taken to be the one at the corner of the unit cell. Since the gold enrichment could have occurred on any of the sublattices, there are four variants. The symmetry of the ordered structure has become that of a primitive cubic lattice. Then the copper atoms preferentially occupy the remaining

*PRESENT ADDRESS: DEPARTMENT OF ENGINEERING SCIENCES AND APPLIED MATHEMATICS, NORTHWESTERN UNIVERSITY, 2145 N. SHERIDAN ROAD, EVANSTON, IL 60208, USA

three sublattices, a lattice complex composed of the cell faces, in which these three sublattices remain equivalent by symmetry. The Cu_3Au phase is an example of $L1_2$ ordering in the Strukturbericht notation system [2]. Another example that we consider here is the $L1_0$ phase, which represents an ordered phase such as CuAu at concentrations near 50% Au; in this case the symmetry breaking splits the four sublattice into two pairs of two equivalent sublattices, and the symmetry of a primitive tetragonal lattice. The ordering results in alternating planes of Cu and Au normal to one of the original cube axes, with six possible variants. In the original FCC unit cell the Cu preferentially occupies the corners and one of the sets of faces, and Au the other two sets faces.

Interfaces can occur between any two variants of the same phase over the range of temperature and concentration where this phase is stable. Interfaces can also occur between any two phases at temperatures where these phases coexist, with the concentrations of the phases dictated by equilibrium conditions as depicted by phase diagrams. In previous work we have examined gradient energy formulations of the diffuse interfaces produced by such order-disorder transitions in FCC alloys [3–5] and HCP alloys [6], the interphase boundaries (IPBs) between an $L1_2$ phase and the disordered FCC phase, and antiphase boundaries (APBs) that separate different variants of the same ordered phase. The formulation permitted the examination of the orientation dependences of the free energy of these interfaces and their mobility. The derivation of these models focussed on obtaining a continuum free energy functional with a form of the gradient energy terms that is consistent with the underlying symmetry of the atomic lattice. However we employed a simplified bulk free energy density that, while it permitted easy calculation of the interface properties, has long been known to give an unrealistic phase diagram [7].

Efforts to compute a phase diagram for an FCC binary alloy date back to Shockley and coworkers [7]; the diagram that resulted from the Bragg-Williams approximation used there was topologically different from, and a poor approximation to, the experimental phase diagram for the prototype Cu–Au system [8]. Many efforts to improve upon the situation followed [2,9,10]; realistic phase diagrams for the Cu–Au system were obtained by using the cluster variation method (CVM) and asymmetric multiparticle interactions [11]. CVM and Monte Carlo (MC) methods have had a number of successes modeling alloy systems of varying complexity; the reader is referred to recent reviews [2, 12] for discussion of those methods.

Thus in the last twenty years it has been possible to obtain a realistic phase diagram from statistical mechanical models, particularly for CVM [2,9,11,13]. CVM models are cumbersome and their existence is often ignored [14]. They have been used to make discrete calculations of the energy of the interfaces (e.g., [13, 15]). But such discrete calculations of interfaces do not lend themselves to studying the orientation dependent properties. In this paper we describe an improved bulk free energy model for the bulk free energy density that allows a more realistic description of the equilibrium phase diagram of the system, but still simple enough to be used for describing the orientation dependence of the energy and motion kinetics of the interfaces. It is our hope that its simplicity will find wider applications.

Our method has elements in common with the sublattice models developed by Sundman, Dupin and others [16–19]. These models have been used successfully

to produce realistic phase diagrams for FCC alloy systems. Their method features many more parameters than our model; in practice, these parameters are determined by fitting experimental measurements of the phase diagram and other thermodynamic quantities, such as the latent heat and heat capacity. Here we show that realistic phase diagrams may also be obtained using our simple model; we anticipate that this simplicity will ultimately be advantageous in the self-consistent calculation of energetic and kinetic anisotropies of phase boundaries.

The paper is organized as follows. The formulation is given in Section 2; the method for finding phase diagrams and some results are given in Section 3. Finally, discussion and conclusions are presented in the last two sections.

2 Formulation

2.1 The Concentration and Order Parameters

We briefly recall the mean-field description of the order-disorder transitions on an FCC lattice given in Ref. [4]. A binary alloy (denoted A–B) on an FCC crystal lattice is described geometrically by four interpenetrating cubic sublattices, with sublattice occupation densities ρ_j defined at the lattice points shown in Fig. 1. The four densities represent the local atomic fraction of species A on each sublattice; their specification is assumed to characterize the overall state of the crystal.

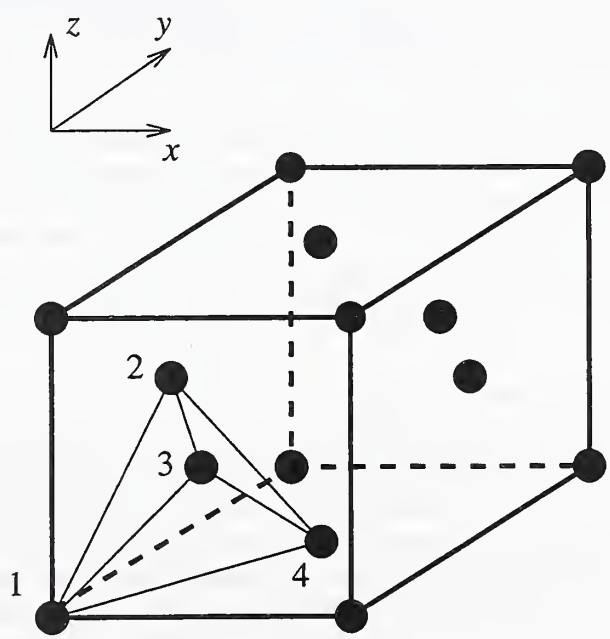

Figure 1. A schematic diagram of an FCC lattice. To describe ordering in this model there are four distinguished sites corresponding to a corner and one each for the faces intersecting at that corner.

It is convenient to introduce four new parameters W, X, Y, and Z defined by

$$W = \frac{1}{4}(\rho_1 + \rho_2 + \rho_3 + \rho_4), \tag{1}$$

$$X = \frac{1}{4}(\rho_1 + \rho_2 - \rho_3 - \rho_4), \tag{2}$$

$$Y = \frac{1}{4}(\rho_1 - \rho_2 + \rho_3 - \rho_4), \tag{3}$$

$$Z = \frac{1}{4}(\rho_1 - \rho_2 - \rho_3 + \rho_4). \tag{4}$$

These relations can be inverted to give

$$\rho_1 = W + X + Y + Z, \tag{5}$$

$$\rho_2 = W + X - Y - Z, \tag{6}$$

$$\rho_3 = W - X + Y - Z, \tag{7}$$

$$\rho_4 = W - X - Y + Z, \tag{8}$$

which can be interpreted in terms of the expression [14]

$$\rho = W + X\cos 2\pi x/a + Y\cos 2\pi y/a + Z\cos 2\pi z/a, \tag{9}$$

which gives the relations (5–8) upon evaluation at the corners and face centers of the conventional unit cell in Fig. 1; here a is the cubic lattice constant. Thus parameter W represents the atomic fraction of the system as a whole, and is a conserved order parameter. X, Y, and Z are non-conserved order parameters that can vary between plus and minus one half, and are Fourier coefficients representing density variations along the directions of the crystal axes.

In this model the disordered state is represented by $\rho_1 = \rho_2 = \rho_3 = \rho_4 = W$, which implies that $X = Y = Z = 0$. Ordered states are characterized by non-zero values for the non-conserved order parameters. For instance, the four equivalent variants of A_3B $L1_2$ ordering are $|X| = |Y| = |Z| \neq 0$ with $XYZ < 0$, and the four variants of AB_3 $L1_2$ ordering are $|X| = |Y| = |Z| \neq 0$ with $XYZ > 0$. The six variants of $L1_0$ ordering are $X = Y = 0$ with $|Z| \neq 0$, $Y = Z = 0$ with $|X| \neq 0$, and $Z = X = 0$ with $|Y| \neq 0$, with layering respectively in the xy, yz, and zx planes. A bulk equilibrium state is characterized by constant values of the densities and order parameters.

2.2 The Thermodynamic Description

A thermodynamic description of the crystal for the case of an isothermal system is based on the bulk Helmholtz free energy density (per mole) $F(X, Y, Z, W, T)$. In Ref. [4], we considered an energy model based on pair-wise interactions, which lead to an unrealistic phase diagram with a multiphase critical point. The problem lies in the positive definiteness of the fourth-order terms in the expansion of the entropic part of F. Pair-wise interaction energies make no contribution to these fourth order terms. In the present work, we develop an improved model for the free energy density, by introducing negative fourth-order contributions to the energy to make the fourth-order free energy terms no longer positive definite. We are then able to obtain a more realistic description of the binary alloy phase diagram.

The idea behind our modification can be motivated by familiar examples from the bifurcation theory of scalar systems [20]. For a fourth-degree free energy density,

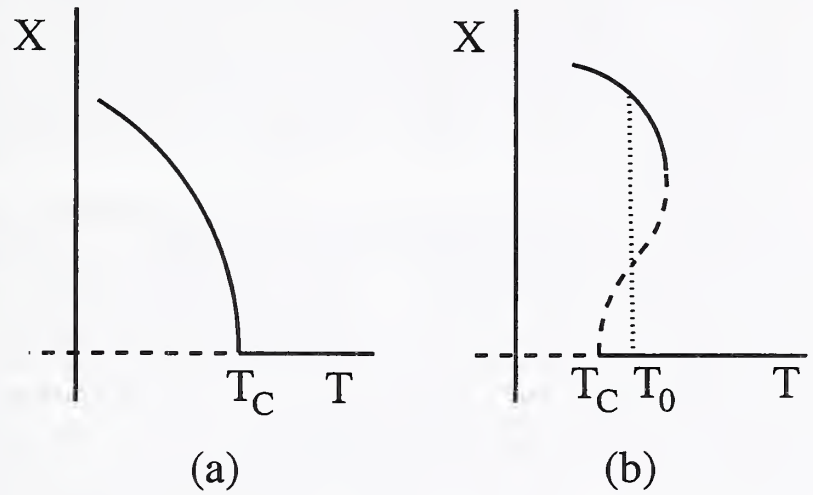

Figure 2. Schematic bifurcation curves for the order parameter X versus the temperature T near a critical point T_c. Stable and unstable solutions are indicated by solid and dashed curves, respectively. (a) A fourth-degree theory results in a second-order phase transition: the disordered state ($X = 0$) changes continuously into the ordered state ($X \neq 0$) at T_c. (b) A sixth-degree theory results in a first-order phase transition: locally stable ordered and disordered states exist on either side of T_0, and have equal energies at T_0 (dotted curve). The order parameter $X(T)$ for the minimum energy state jumps discontinuously as the temperature passes through T_0.

at $W = 1/2$ the $L1_0$ ordering is a second-order phase transition in which the order parameter changes continuously from zero to non-zero values as the temperature passes through its critical value T_c. A scalar model with $Y = Z = 0$ for the free energy density of the $L1_0$ transition is

$$F(W,X,T) = f_0(W,T) + f_2(W,T)X^2 + f_4(W,T)X^4, \qquad (10)$$

with $f_4(1/2,T) > 0$ and $f_2(1/2,T) \sim (T - T_c)$. For $T \geq T_c$ the system is in stable equilibrium for the disordered state $X = 0$, whereas for $T < T_c$ the lowest energy state is an ordered phase with $X^2 = -f_2/(2f_4)$. The ordered and disordered states are never simultaneously stable, as illustrated in Fig. 2a. A first-order phase transition can be obtained from a sixth-order model such as

$$F(W,X,T) = f_0(W,T) + f_2(W,T)X^2 + f_4(W,T)X^4 + f_6(W,T)X^6, \qquad (11)$$

where $f_2(1/2,T) \sim (T - T_c)$ as before, but now $f_4(1/2,T) < 0$ and $f_6(1/2,T) > 0$. In this case, as illustrated in Fig. 2b, the minimum energy state changes discontinuously from a disordered phase to an ordered phase with $X^2 = -f_4/(2f_6)$ at the temperature $T_0 > T_c$ for which $f_2 = f_4^2/(4f_6)$.

A simplified model [4] that includes the $L1_2$ transition with $|X| = |Y| = |Z| \neq 0$ involves in addition a cubic term $f_3(W,T)XYZ$. The coefficient $f_3(W,T)$ of the third order term in the free energy expansion depends strongly on the composition,

and in a symmetric model is antisymmetric about $W = 1/2$, and equals 0 there. At compositions on either side of $W = 1/2$, the sign of XYZ can always be chosen to make the term $f_3(W,T)XYZ$ negative, with $X = \pm Y = \pm Z$. Thus in a fourth-degree theory, $L1_2$ is always favored over $L1_0$ near the critical point T_c, except exactly at $W = 1/2$. In a sixth-degree theory with negative-definite fourth-order terms, the $L1_0$ transition is first order and has a critical point at $T_0 > T_c$. The energy differences between the $L1_0$ and $L1_2$ phases at the lower temperature T_c are then unimportant, and the $L1_0$ phase can be favored over the $L1_2$ phase near $W = 1/2$ and $T = T_0$.

The free energy model used in our previous work featured a fourth-degree polynomial expansion with positive definite fourth-order coefficients. This expansion was adequate for the description of the $L1_2$ transition near $W = 1/4$, but necessarily lead to a multicritical point at $W = 1/2$ and a second-order phase transition for the $L1_0$ structure, whose temperature dependence is similar to Fig. 2a. Our improved models in this paper are based on four-atom interactions in the energy which add negative fourth-order terms of a large enough magnitude to make the fourth-order term negative in a polynomial expansion at $W = 1/2$. As before the sixth-degree terms result entirely from the entropy and are positive. The main goal of the present work is to extend the model to higher degree in order to obtain a more realistic treatment of all the transitions, and to find appropriate choices for the dependence of the free energy density on temperature and concentration so that realistic phase diagrams for these order-disorder transitions can be obtained. There are enough parameters in a four-atom interaction model to affect the behavior when $W \neq 1/2$.

In the next two subsections, we describe the models of the internal energy density E and entropy S that are used to obtain the improved free energy density $F = E - TS$ that we use in this work.

2.3 The Internal Energy

The internal energy per mole, E, of the system is assumed to be characterized by four-atom cluster energies E_{40}, E_{31}, E_{22}, E_{13}, and E_{04} of the various occupations of the near-neighbor basic tetrahedral form by A_4, A_3B, A_2B_2, AB_3, and B_4, respectively, that allow for four-particle interactions according to the scheme [11]

$$\begin{aligned} E = {} & E_{40}\rho_1\rho_2\rho_3\rho_4 + E_{31}\left[\rho_1\rho_2\rho_3(1-\rho_4) + \rho_1\rho_2(1-\rho_3)\rho_4 + \right. \\ & \left. \rho_1(1-\rho_2)\rho_3\rho_4 + (1-\rho_1)\rho_2\rho_3\rho_4\right] + \\ & E_{22}\left[\rho_1\rho_2(1-\rho_3)(1-\rho_4) + \rho_1(1-\rho_2)\rho_3(1-\rho_4) + \right. \\ & \left. \rho_1(1-\rho_2)(1-\rho_3)\rho_4 + +(1-\rho_1)(1-\rho_2)\rho_3\rho_4 \right. \\ & \left. + (1-\rho_1)\rho_2(1-\rho_3)\rho_4 + (1-\rho_1)\rho_2\rho_3(1-\rho_4)\right] \\ & + E_{13}\left[\rho_1(1-\rho_2)(1-\rho_3)(1-\rho_4) + (1-\rho_1)\rho_2(1-\rho_3)(1-\rho_4)\right. \\ & \left. + (1-\rho_1)(1-\rho_2)\rho_3(1-\rho_4) + (1-\rho_1)(1-\rho_2)(1-\rho_3)\rho_4\right] \\ & + E_{04}(1-\rho_1)(1-\rho_2)(1-\rho_3)(1-\rho_4). \end{aligned} \tag{12}$$

By substituting Eqns. (5–8) into the above expression, we obtain an internal energy of the form

$$E = e_0 + e_2(X^2 + Y^2 + Z^2) + e_3XYZ + e_{41}(X^4 + Y^4 + Z^4) + e_{42}(X^2Y^2 + X^2Z^2 + Y^2Z^2), \tag{13}$$

and the e_i are given in the appendix in terms of E_{40}, E_{31}, E_{22}, E_{13} and E_{04}.

2.4 Entropy approximations

The point approximation to the molar entropy S of the system is given by the expression

$$S(\rho_1, \rho_2, \rho_3, \rho_4) = -\frac{R}{4}\sum_{j=1}^{4} \mathcal{I}(\rho_j), \tag{14}$$

where

$$\mathcal{I}(x) = x\ln(x) + (1-x)\ln(1-x) \tag{15}$$

and R is the ideal gas constant. This expression for the entropy is the sum of the contribution from each sublattice.

We explore two choices based on Eqn. (14). One option is to use the expression as is, which is somewhat complicated by the presence of the logarithmic terms, which generally forces one to compute numerical solutions to the problem. Another option is to expand this expression in a power series about the points $\rho_j = 1/2$, and truncate the series after sixth degree. The result allows more progress to be made analytically.

$$S = \frac{-R}{4}\sum_{j=1}^{4}\left\{-\log 2 + 2(\rho_j - \frac{1}{2})^2 + \frac{4}{3}(\rho_j - \frac{1}{2})^4 + \frac{32}{15}(\rho_j - \frac{1}{2})^6 + \mathcal{O}(\rho_j - \frac{1}{2})^8\right\}. \tag{16}$$

Inserting the definitions (5–8) into this expression results in polynomial expressions involving $U = W - 1/2$ and the order parameters X, Y, Z up to sixth degree.

2.5 Free Energy Approximations

The form of the Helmholtz free energy density, $F = E - TS$, follows from Eqn. (13), and is given by an expression of the form

$$\begin{aligned} F(X,Y,Z,W,T) = {} & e_0 + e_2(X^2 + Y^2 + Z^2) + \\ & e_3XYZ + e_{41}(X^4 + Y^4 + Z^4) + \\ & e_{42}(X^2Y^2 + X^2Z^2 + Y^2Z^2) + \frac{RT}{4}\sum_{j=1}^{4}\mathcal{I}(\rho_j). \end{aligned} \tag{17}$$

where we must use Equations (5–8) to get the entropy contribution in terms of the order parameters. Using Eqn. (16) the resulting approximation for the free energy

takes the form

$$\begin{aligned} F(X,Y,Z,W,T) = {} & f_0 + f_2(X^2+Y^2+Z^2) + f_3XYZ + \\ & f_{41}(X^4+Y^4+Z^4) + f_{42}(X^2Y^2+X^2Z^2+Y^2Z^2) + \\ & f_{51}XYZ(X^2+Y^2+Z^2) + f_{61}(X^6+Y^6+Z^6) + \\ & f_{62}[X^4(Y^2+Z^2)+Y^4(X^2+Z^2)+Z^4(X^2+Y^2)] + \\ & f_{63}X^2Y^2Z^2, \end{aligned} \tag{18}$$

where the coefficients f_i, for parameter choices suggested by those of Kikuchi and de Fontaine [11] discussed above, are given in the appendix. In Section 4.1 we shall give the results for a phase diagram using this polynomial approximation.

3 Phase diagrams

A phase diagram consists of curves in the temperature-concentration plane that describe conditions for equilibrium between various bulk phases at the same temperature, but not necessarily at the same concentration. Mathematically, this is a minimization of the free energy subject to a fixed amount of the total amount of concentration W in the system, which results in a common tangent construction in terms of the free energy of the system [21]. The free energy is also an unconstrained minimum with respect to the non-conserved order parameters X_j. This procedure produces several sets of equations to solve for the concentration between stable bulk phases that delineate regions where two or more phases can coexist. To describe the computation of phase diagrams, we first discuss the bulk equilibrium states that are supported by the model.

3.1 Bulk Phases

In the case of the disordered FCC phase, we have $X = Y = Z = 0$; for high enough temperatures this will occur for any overall concentration W. We denote the resulting free energy for the bulk FCC phase by $F_{FCC}(W,T)$; for the case in Eqn. (17), we then have

$$F_{FCC}(W,T) \equiv F(0,0,0,W,T) = e_0(W) + RT\,[\mathcal{I}(W)]\,. \tag{19}$$

For the $\mathrm{L1_0}$ variant with $Z \neq 0$, the corresponding free energy $F_{L1_0}(Z,W,T)$ becomes

$$\begin{aligned} F_{L1_0}(Z,W,T) \equiv F(0,0,Z,W,T) = {} & e_0(W) + e_2(W)Z^2 + e_{41}Z^4 + \\ & \frac{RT}{2}\,[\mathcal{I}(W+Z) + \mathcal{I}(W-Z)] \end{aligned} \tag{20}$$

for this phase.

Finally, for the $\mathrm{L1_2}$ variant with $X = Y = Z \neq 0$ the free energy $F_{L1_2}(Z,W,T)$ becomes

$$\begin{aligned} F_{L1_2}(Z,W,T) \equiv F(Z,Z,Z,W,T) = {} & e_0(W) + 3e_2(W)Z^2 \\ & + e_3(W)Z^3 + 3(e_{41}+2e_{42})Z^4 + \\ & \frac{RT}{4}\,[\mathcal{I}(W+3Z) + 3\mathcal{I}(W-Z)]\,. \end{aligned} \tag{21}$$

3.2 *FCC–$L1_0$ Transition*

Conditions under which an equilibrium between the disordered FCC phase and the ordered $L1_0$ phase can coexist are described by the system of nonlinear equations

$$\frac{\partial F_{L1_0}}{\partial Z}(Z_0, W_0) = 0, \tag{22}$$

$$\frac{\partial F_{L1_0}}{\partial W}(Z_0, W_0) = \frac{\partial F_{FCC}}{\partial W}(W_{FCC}) = \mu_0, \tag{23}$$

and

$$F_{FCC}(W_{FCC}) - F_{L1_0}(Z_0, W_0) - \mu_0 (W_{FCC} - W_0) = 0, \tag{24}$$

for a given T. Eqn. (22) results from minimizing the free energy with respect to Z, and Eqn. (22) is the result of minimizing with respect to W subject to a specified overall concentration, leading the appearance of the Lagrange multiplier μ_0. Eqn. (24) completes the common tangent construction, and expresses the fact that the energy is also stationary with respect to variations in the interface position. The unknowns in these equations are the concentration of the disordered phase W_{FCC} and the concentration and order parameter of the $L1_0$ phase, W_0 and Z_0, respectively. These equations were solved using DNSQ [22,23] using suitable initial guesses. These guesses were generated from the T_0 curve, which is in turn found by setting the free energies of the two phases equal and requiring $\partial F/\partial Z = 0$. This strategy was used in all cases where there was coexisting ordered and disordered states.

3.3 *FCC–$L1_2$ Transition*

In this case, we must satisfy the system of nonlinear equations

$$\frac{\partial F_{L1_2}}{\partial Z}(Z_2, W_2) = 0 \tag{25}$$

$$\frac{\partial F_{L1_2}}{\partial W}(Z_2, W_2) = \frac{\partial F_{FCC}}{\partial W}(W_{FCC}) = \mu_2, \tag{26}$$

and

$$F_{FCC}(W_{FCC}) - F_{L1_2}(Z_2, W_2) - \mu_2 (W_{FCC} - W_2) = 0, \tag{27}$$

for a given T. The unknowns are the concentration of the disordered phase W_{FCC} and the concentration and order parameter of the $L1_2$ phase, W_2 and Z_2 respectively.

3.4 *$L1_0$–$L1_2$ Transition*

In this final case, we must satisfy the system of nonlinear equations

$$\frac{\partial F_{L1_0}}{\partial Z}(Z_0, W_0) = 0 \tag{28}$$

$$\frac{\partial F_{L1_2}}{\partial Z}(Z_2, W_2) = 0 \tag{29}$$

$$\frac{\partial F_{L1_0}}{\partial W}(Z_0, W_0) = \frac{\partial F_{L1_2}}{\partial W}(Z_2, W_2) = \mu_1, \tag{30}$$

and

$$F_{L1_0}(Z_0, W_0) - F_{L1_2}(Z_2, W_2) - \mu_1 (W_0 - W_2) = 0, \tag{31}$$

for a given T. The unknowns are the concentrations and order parameters for the respective ordered phases.

4 Results

We next present results of numerically-computed phase diagrams using these equations. The results are given in non-dimensional form by using the energy scale $-\omega$ to nondimensionalize the free energies and the temperature scale $-\omega/R$ to nondimensionalize T.

4.1 Results Using the Sixth-Degree Landau Expansion

We first describe a phase diagram based on the free energy function given in Eqn. (18), using the parameters

$$f_0(U,T) = -\frac{9}{2} + 6U^2 + T(\ln\frac{1}{2} + 2U^2), \tag{32}$$

$$f_2(U,T) = -4 + 40U^2 + 2T, \tag{33}$$

$$f_3(U) = -250(U - \alpha U^3), \tag{34}$$

$$f_{41} = -4, \tag{35}$$

$$f_{42} = \beta, \tag{36}$$

$$f_{61} = 4, \tag{37}$$

$$f_{62} = -3, \tag{38}$$

$$f_{63} = 6, \tag{39}$$

where $U = W - 1/2$. With the choice $\alpha = 2$ and $\beta \approx 27.735894$, we will have equal dimensionless temperatures of $T = 2.5$ at the congruent points of the FCC–$L1_2$ and FCC–$L1_0$ order-disorder transitions near $W = 1/4$ and $W = 1/2$, respectively. The choice of the last two parameters, f_{62} and f_{63}, in the free energy function (18) was made so that the sixth degree terms would drop out of the problem when $X = Y = Z$ and leave the analysis of the bulk $L1_2$ phase unaffected.

By solving the required nonlinear equations using the sixth-degree polynomial form and these coefficients, we arrive at the phase diagram shown in Fig. 3. This phase diagram is an idealized, symmetric approximation to the CuAu binary system [8]. The choice $-\omega/R \approx 265$K would locate the congruent points at about the right temperatures for CuAu. The qualitative appearance of the phase diagram for temperatures in the vicinity of the congruent points is satisfactory, but the behavior of the system in the dilute limit is unrealistic. The situation is improved by retaining the logarithmic terms in the entropy contribution to the free energy density, and we focus our attention on this model in the remainder of the paper.

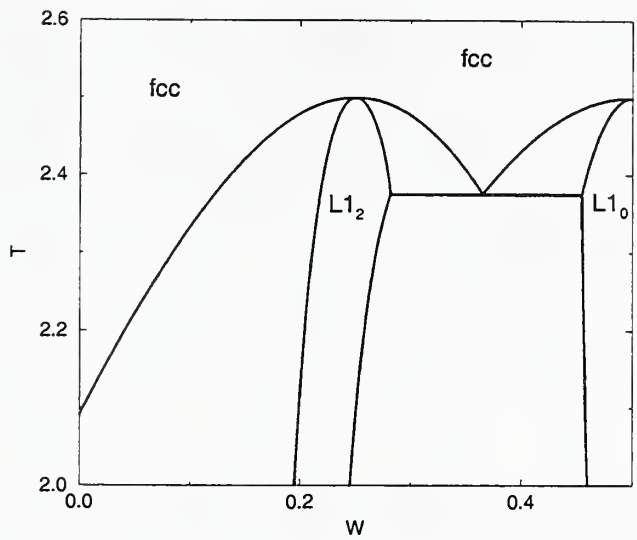

Figure 3. A model phase diagram for the Cu–Au system, from the parameters listed in Eqn. (32). Note that it is symmetric about $W = 1/2$.

Table 1. Coefficients used for the internal energy contribution to the free energy density; here $U = W - 1/2$.

Case	I	II	III
$e_0(U)$	$6U^2$	$6U^2$	$6U^2$
$e_2(U)$	$-4 + U^2$	$-4 + U^2$	$-4 + U^2$
$e_3(U)$	$200U(1 - 2U^2)$	$200U(1 - 2U^2)$	$100U(1 - 2U^2)$
e_{41}	-12	-5	-12
e_{42}	15	10	15

4.2 Results Using the Free Energy with Logarithmic Terms

We next discuss examples of phase diagrams obtained by using the free energy model given by Eqn. (17) with coefficients given in Table 1. The first case is a qualitative model for the Cu–Au system, and the last two are for demonstration purposes. We note that with these coefficients, the limit of metastability for the disordered phase for $W = 1/2$ (corresponding to the temperature T_c in Fig. 2b) occurs at a dimensionless temperature $T = 2$ in all three cases.

With the coefficients of case I, the phase diagram in Fig. 4 is obtained. This diagram is qualitatively similar to that for the Cu-Au system [8], but with symmetry about $W = 1/2$. This model diagram should be sufficient for the purposes of studying the surface tension anisotropy of IPBs in our future work.[a]

[a] In order to obtain quantitative agreement with the congruent point of the FCC-L1$_2$ transition,

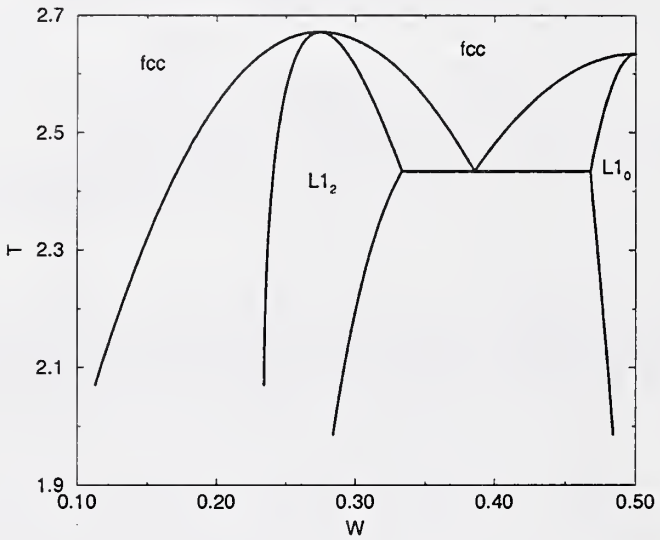

Figure 4. A model phase diagram for the Cu–Au system, from the parameters of Case I. Note that it is symmetric about $W = 1/2$.

For the parameters of Case II, we find that the phase diagram has a lowered and substantially reduced region where the FCC–$L1_0$ transition occurs; see Fig. 5. From Fig. 5 we can see that the coexistence region for the FCC and $L1_0$ phases is dramatically smaller than for case I. As e_{41} rises toward the value $-8/3$, the FCC–$L1_0$ transition region disappears and becomes a multicritical point at $e_{41} = -8/3$.

The phase diagram for the parameters of case III is given in Fig. 6. In this case, the congruent point for the FCC–$L1_2$ transition is just outside the FCC–$L1_0$ coexistence region; further decrease in e_3 will result in a peritectoid phase diagram.

We can summarize the effects of the parameters as follows. The size of e_3 controls the location of the congruent point for the FCC–$L1_2$ transition. If it is sufficiently large, then the congruent point is shifted to values symmetrically located about $W = 1/2$ with temperature greater than 2. The value of e_{41} controls the location of the congruent point for the FCC–$L1_0$ transition. If $e_{41} < -8/3$, the congruent point remains at $W = 1/2$ but occurs at $T > 2$. If $e_{41} > -8/3$, the congruent point is at $T = 2$ and the transition is second order. Using these parameters we have been able to obtain satisfactory phase diagrams that would allow the description of the variation of concentration across both interphase and antiphase boundaries.

---

we would choose $-\omega/R \approx 248$K.

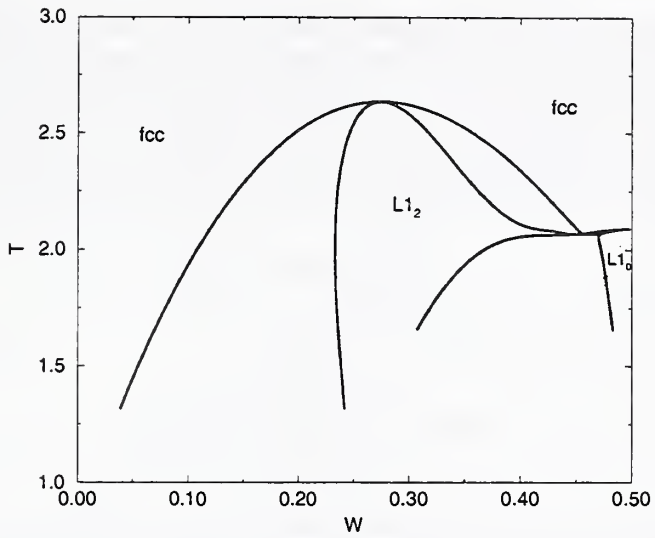

Figure 5. The phase diagram from the parameters of Case II. The region where $L1_0$ is the sole stable phase is near $(W, T) = (0.5, 2)$. The multicritical point at $e_{41} = -8/3$ is being approached, and the FCC-$L1_0$ transition is disappearing.

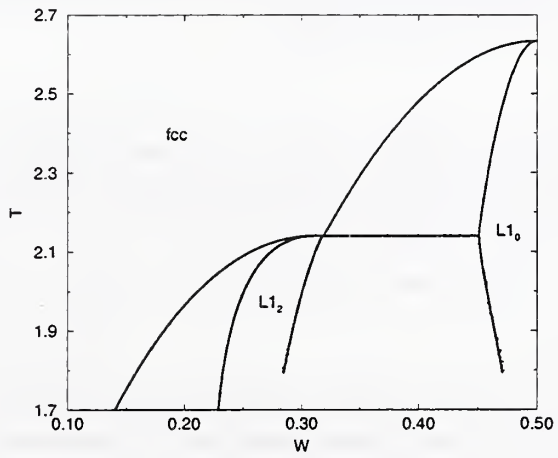

Figure 6. The phase diagram from the parameters of Case III.

5 Discussion

The solutions to the nonlinear equations that give the curves on the phase diagram become difficult to compute when the dimensionless temperature drops below about 2 for the case with logarithmic terms in the entropy. The difficulty appears to be that the values of the order parameters and concentration are approaching the limits of the ranges allowed by the logarithmic terms. For example, in the free energy density for the $L1_2$ phase, there is a term in the argument of the ln function that requires

$$1 - W - 3Z > 0; \tag{40}$$

solving for Z gives

$$Z < \frac{1 - W}{3}. \tag{41}$$

From the $L1_0$ phase, we can also conclude that we must have

$$W > Z. \tag{42}$$

We may plot the boundaries of these inequalities along with the solutions to the nonlinear equations that give the phase diagram in the (W, Z)-plane; this has been done in Fig. 7. The temperature is decreasing as the solid curves (representing the coexistence region boundaries) approach the edges of their allowed ranges (dashed lines). The jumps in slope occur at the ends of the tie line at the eutectoid temperature for Case I. We hypothesize that when the solutions get too close to these boundaries, the iteration procedure breaks down because the procedures allow iterates beyond the boundaries. We believe that we can recast the equations to eliminate the logarithmic terms and thus alleviate this problem; this is allowed by the special form of the free energy density.

6 Conclusion

We have been able to compute a simple model phase diagram with an approach that is a modification to the quasi-chemical description. The modifications were rooted in the choices of Kikuchi and coworkers [11, 15] in their successful CVM approaches, but we have modified the coefficients to suit our needs in drawing the phase diagram. We found that two coefficients (e_3 and e_{41}) in the internal energy contribution to the free energy made the biggest contributions to controlling the resulting phase diagram.

The coefficient e_{41} of the terms involving X_i^4 strongly affects the temperature of the congruent point for the FCC-$L1_0$ transition; there is a multicritical point at $e_{41} = -8/3$, at which the first order nature of the transition disappears. Elsewhere we will show that as one approaches the multicritical point for the FCC–$L1_0$ phase transition, there is a quadratic decay in the interfacial energy of the interphase boundaries for any orientation [24].

The size of the coefficient e_3 plays a crucial role in setting the temperature and concentration of the congruent point in the FCC-$L1_2$ transition. When it is larger, the congruent point occurs at larger temperatures. When it decreases, the

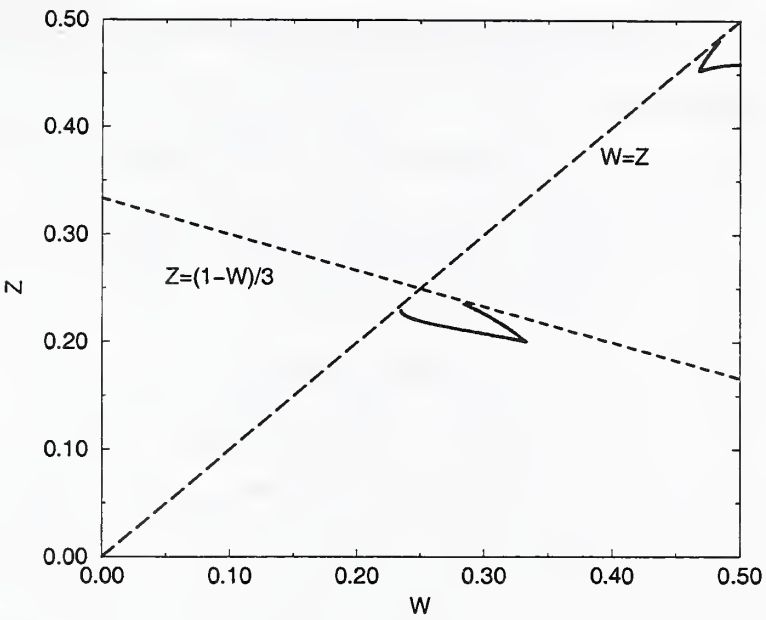

Figure 7. The dashed lines show the limits of the allowed ranges for the arguments of the ln functions. The solid curves are plots of the order parameters found along the coexistence region boundaries for the parameters of Case I. The lower curves near the middle of the plot are for the $L1_2$ boundaries and the curves in the upper right are for the $L1_0$ boundaries.

congruent point disappears inside the FCC-$L1_0$ coexistence region and a peritectoid phase diagram occurs. We have not yet computed the peritectoid phase diagram due to numerical difficulties with the logarithmic terms; recasting the root-finding procedure to eliminate these terms should alleviate this difficulty.

7 Acknowledgements

It is a pleasure to dedicate this paper to S.H. Davis on the occasion of his sixtieth birthday, and to acknowledge the tremendous influence of his research and his friendship on the many students and colleagues that have had the good fortune of associating with him.

The authors are also grateful for helpful discussions with S. Langer and W.J. Boettinger during the preparation of this manuscript. This research was conducted with the support of the Microgravity Research Division of NASA and the University of Delaware Research Foundation.

Appendix

If we begin with Eqn. (12), and substitute the expressions (5–8) to eliminate the occupation densities ρ_i, we obtain the expression

$$\begin{aligned}
E = \frac{1}{16}&[4E_{31} + 6E_{22} + 4E_{13} + E_{04} + E_{40}] + U[E_{31} - E_{13} - E_{04}/2 + E_{40}/2] \\
&+ U^2[3E_{40}/2 - 3E_{22} + 3E_{04}/2] + U^3[-4E_{31} + 4E_{13} - 2E_{04} + 2E_{40}] \\
&+ U^4[-4E_{31} + 6E_{22} - 4E_{13} + E_{04} + E_{40}] \\
&+ (X^2 + Y^2 + Z^2)\{E_{22} - E_{40}/2 - E_{04}/2 + U[4E_{31} - 4E_{13} + 2E_{04} - 2E_{40}] \\
&+ U^2[8E_{31} - 12E_{22} + 8E_{13} - 2E_{04} - 2E_{40}]\} \\
&+ XYZ\{-8E_{31} + 8E_{13} - 4E_{04} + 4E_{40} \\
&+ U[-32E_{31} + 48E_{22} - 32E_{13} + 8E_{04} + 8E_{40}]\} \\
&+ (X^2Y^2 + X^2Z^2 + Y^2Z^2)\{8E_{31} - 12E_{22} + 8E_{13} - 2E_{04} - 2E_{40}\} \\
&+ (X^4 + Y^4 + Z^4)\{-4E_{31} + 6E_{22} - 4E_{13} + E_{04} + E_{40}\}, \qquad (43)
\end{aligned}$$

where $U = W - 1/2$. We note that if $E_{40} = E_{31} = E_{22} = E_{13} = E_{04} = 1$, then $E = 1$.

A simple bond counting argument is based on the bond energies E_{AA}, E_{AB} and E_{BB} between the A–A, A–B, and B–B pairs of atoms, respectively. If we assume that $E_{AA} = E_{BB}$ and use a reference energy corresponding to E_{AA}, then the energies of the different configurations according to this scheme are

$$E_{40} = 0, \quad E_{31} = 3\omega, \quad E_{22} = 4\omega, \quad E_{13} = 3\omega, \quad E_{04} = 0, \qquad (44)$$

where $\omega = E_{AB} - E_{AA}$, so that the configurational energies are thus characterized in terms of the energy ω. Substituting these expressions into Eqn. (43) gives that

$$E = E_0 + 4\omega[X^2 + Y^2 + Z^2]. \qquad (45)$$

This expression for the internal energy density is inadequate for the purposes of drawing phase diagrams [7].

A better model for the multiparticle interactions in the internal energy, as given by Kikuchi and de Fontaine [11] and used in Kikuchi and Cahn [15], is to take

$$E_{40} = 0, \quad E_{31} = 3\omega(1 + a), \quad E_{22} = 4\omega, \quad E_{13} = 3\omega(1 + b), \quad E_{04} = 0. \qquad (46)$$

where the constants a, b and ω were determined from a best fit to the phase diagram for the case of Cu–Au system:

$$a = 0.01, \quad b = -0.08, \quad \frac{\omega}{R} = -663\ K. \qquad (47)$$

With this scheme we obtain more terms in the internal energy density of Eqn. (13), and the coefficients e_i in that expression are given by

$$\begin{aligned}
e_0 &= \frac{3}{2}\omega(U^2 - 1/4)\left[4 + a + b + 4(a - b)U + 4(a + b)U^2\right] \\
e_2 &= 2\omega + 6\omega U[a - b + 2(a + b)U] \\
e_3 &= 12\omega(a + b)[b - a - 4(a + b)U], \\
e_{41} &= -6\omega(a + b), \quad e_{42} = 12\omega(a + b). \qquad (48)
\end{aligned}$$

These expressions are used to motivate the choices made for the energy coefficients shown in table 1.

For the polynomial free energy (18) we have the coefficients

$$
\begin{aligned}
f_0 &= \frac{3}{2}\omega\left\{(U^2-1/4)\left[4+a+b+4(a-b)U+4(a+b)U^2\right]\right\} \\
&\quad +RT\left(2U^2+\frac{4}{3}U^4+\frac{32}{15}U^6+\ln(1/2)\right) \\
f_2 &= 2\omega+\omega U[a-b+2(a+b)U]+RT\left[2+8U^2+32U^4\right], \\
f_3 &= 12\omega[b-a-4(a+b)U]+RT\left[32U+256U^3\right], \\
f_{41} &= -6\omega(a+b)+RT\left[\frac{4}{3}+32U^2\right], \\
f_{42} &= 12\omega(a+b)+RT\left[8+192U^2\right],
\end{aligned}
$$

$$
f_{51} = 256RTU, \quad f_{61} = 32RT/15, \quad f_{62} = 32RT, \quad f_{63} = 192RT, \tag{49}
$$

and $R = kN_0$ is the gas constant, where N_0 is Avogadro's number. These expressions are used to motivate the choices made for the energy coefficients shown in Eqns. (32–39).

References

1. J.W. Christian, *The Theory of Transformations in Metals and Solids*, Part I (Pergamon Press, Oxford, 1975).
2. F. Ducastelle, *Order and Phase Stability in Alloys*, (North-Holland, New York, 1991).
3. R.J. Braun, J.W. Cahn, J. Hagedorn, G.B. McFadden and A.A. Wheeler, in *Mathematics of Microstructure Evolution*, ed. L-Q. Chen *et al.*, (TMS/SIAM, Philadelphia, 1996) 225.
4. R.J. Braun, J.W. Cahn, G.B. McFadden, and A.A. Wheeler, *Trans. Roy. Soc. London A* **355**, 1787 (1997).
5. R.J. Braun, J.W. Cahn, G.B. McFadden, H.E. Rushmeier and A.A. Wheeler, *Acta mater.* **46**, 1 (1997).
6. J.W. Cahn, S. Han, and G.B. McFadden, *J. Stat. Phys.* **95**, 1337 (1999).
7. Nix, F.C. and and Shockley, W. *Rev. Mod. Phys.* **10**, 1 (1938).
8. H. Okamoto, D.J. Chakrabarti, D.E. Laughlin and T.B. Massalski, *Bull. Alloy Phase Diagrams* **8**, 454 (1987).
9. R. Kikuchi, *Prog. Theo. Phys. Supp.* **87**, 69 (1986).
10. R. Kikuchi and H. Sato, *Acta Metall.* **22**, (1974) 1099.
11. R. Kikuchi and D. de Fontaine, *Application of Phase Diagrams in Metallurgy and Ceramics*, ed. by C.G. Carter, NBS Special Publication 496, (1978) p. 967.
12. D. de Fontaine, *Solid State Phys.* **47**, 33 (1994).
13. A. Finel, in *Ordering and Disordering in Alloys*, ed. A. Yavari, (Elsevier Applied Science, New York, 1992) 182.
14. A.G. Khachaturyan, Prog. Mater. Sci. **22**, 1 (1978).
15. R. Kikuchi, and J. W. Cahn, *Acta Metall.* **27**, 1337 (1979).

16. I. Ansara, B. Sundman, and P. Wilemin, *Acta metall. mater.* **36**, 977 (1988).
17. N. Dupin, Contribution à l'évaluation thermodynamique des alliages polyconstitués à base de nickel. Ph. D. Thesis, Laboratoire de Thermodynamique et de Physico-Chimie Métallurgiques de Grenoble, Institut National Polytechnique de Grenoble (1995).
18. I. Ansara, N. Dupin, H.L. Lukas, and B. Sundman, *Journal of Alloys and Compounds* **247**, 20 (1997).
19. B. Sundman, S.G. Fries, and W.A. Oates, *Calphad* **22**, 335 (1998).
20. S.-N. Chow and J.K. Hale, *Methods of Bifurcation Theory*, (Springer-Verlag, Berlin, 1982).
21. P. Haasen, *Physical Metallurgy*, 3rd ed, (Cambridge University Press, 1996).
22. SLATEC Common Math Library, National Energy Software Center, Argonne National Laboratory, Argonne, IL. The program SNSQ was written by K.L. Hiebert and is based on an algorithm of Powell [23].
23. M.J.D. Powell, "A hybrid method for nonlinear equations," in *Numerical Methods for Nonlinear Algebraic Equations*, P. Rabinowitz, ed. (Gordon and Breach, 1988).
24. G. Tanoğlu, R.J. Braun, J.W. Cahn, G.B. McFadden and A.A. Wheeler, in preparation.